

Analysis of thermal properties of GaInN light-emitting diodes and laser diodes

Qifeng Shan, Qi Dai, Sameer Chhajed, Jaehee Cho, and E. Fred Schubert^{a)}

Department of Physics, Applied Physics and Astronomy and Department of Electrical, Computer, and Systems Engineering, Future Chips Constellation, Rensselaer Polytechnic Institute, Troy, New York 12180, USA

(Received 29 June 2010; accepted 24 August 2010; published online 19 October 2010)

The thermal properties, including thermal time constants, of GaInN light-emitting diodes (LEDs) and laser diodes (LDs) are analyzed. The thermal properties of unpackaged LED chips are described by a single time constant, that is, the thermal time constant associated with the substrate. For unpackaged LD chips, we introduce a heat-spreading volume. The thermal properties of unpackaged LD chips are described by a single time constant, that is, the thermal time constant associated with the heat spreading volume. Furthermore, we develop a multistage $R_{th}C_{th}$ thermal model for packaged LEDs. The model shows that the transient response of the junction temperature of LEDs can be described by a multiexponential function. Each time constant of this function is approximately the product of a thermal resistance, R_{th} , and a thermal capacitance, C_{th} . The transient response of the junction temperature is measured for a high-power flip-chip LED, emitting at 395 nm, by the forward-voltage method. A two stage $R_{th}C_{th}$ model is used to analyze the thermal properties of the packaged LED. Two time constants, 2.72 ms and 18.8 ms are extracted from the junction temperature decay measurement and attributed to the thermal time constant of the LED GaInN/sapphire chip and LED Si submount, respectively. © 2010 American Institute of Physics. [doi:10.1063/1.3493117]

I. INTRODUCTION

Presently, III–V nitride based light-emitting diodes (LEDs) are in great demand, due to new markets such as retrofit LED lighting and liquid crystal display backlighting. Self-heating of LEDs is an important issue that affects the internal quantum efficiency, external quantum efficiency and reliability.¹ Several junction-temperature measurement methods have been reported, including the forward-voltage method² and the spectral-shift electroluminescence method.³ Using the forward-voltage method, the junction temperature has been measured under continuous wave conditions.² Using the forward-voltage method, the transient junction temperature after the LED current is switched on or off has been measured as well.⁴ The origin of thermal time constants is found in the thermal storage capacitance and the thermal resistance by which the thermal capacitance is connected to a heat source. Using time-domain⁴ and frequency-domain⁵ measurements, the thermal time constant of LED chips reported in the literature ranges between 1 and 7 ms; for laser diode (LD) chips, a thermal time constant reported in the literature is about 1 μ s.^{6,7} The study of thermal time constants is useful because it reveals the dynamic thermal behavior of a device and provides information on the thermal structure of the device.

High-power GaInN flip-chip packaged LEDs are widely used due to their advantages in thermal management and light-extraction.⁸ In the present study, by using an $R_{th}C_{th}$ model, we analyze different thermal time constants of GaInN

LEDs and LDs. The transient junction temperature of a high-power packaged GaInN flip-chip LED is measured and the thermal properties of the LED are analyzed.

In Sec. II, the thermal time constants of an LED and an LD at the chip level are calculated. The thermal time constant of a GaInN LED chip is determined by using the thermal resistance and the thermal capacitance of the substrate and found to be on the order of millisecond (ms). For a GaInN LD, the thermal time constant is on the order of microsecond (μ s), which is determined by the heat spreading volume. In Sec. III, we analyze the thermal properties of a typical packaged GaInN LED and develop a multistage $R_{th}C_{th}$ model. The transient junction temperature is expressed as a multiexponential function with each time constant associated with a specific R_{th} and C_{th} . Section IV briefly presents experimental procedures of the transient junction temperature measurement. Section V presents experimental results and analyzes them using the theoretical model developed in prior sections. Major conclusions are summarized in Sec. VI.

II. THERMAL TIME CONSTANTS OF AN LED AND AN LD AT THE CHIP LEVEL

Figures 1(a) and 1(b) show a hypothetical circular LED chip and a hypothetical circular LD chip, respectively. A circular geometry is chosen to keep the calculation simple while capturing the essence of the heat flow. With good approximation, the basic results that will be obtained should also be applicable to square-shaped chips having the same area as the circular chips. Due to nonradiative recombination and resistive losses, heat is generated in the active region of an LED. Transfer of heat from the active region to the sub-

^{a)}Electronic mail: efschubert@rpi.edu.

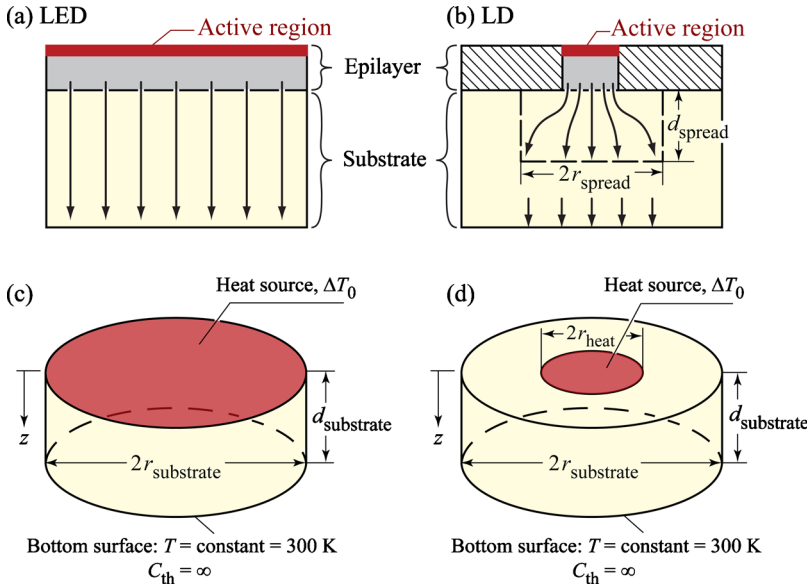


FIG. 1. (Color online) Heat dissipation in (a) an LED and (b) an LD at chip level and schematic illustration of (c) the circular LED and (d) the circular LD on a substrate.

strate occurs by means of thermal conduction; transfer of heat to air occurs by means of thermal convection. Due to the high thermal resistance between the active region and air, the thermal energy mostly transfers from the active region to the substrate. We therefore neglect heat transfer from the active region to air and this will be assumed throughout our study. An LED's active region has approximately the same area as the LED chip, while an LD's active region, e.g., the active region of a vertical-cavity-surface-emitting laser, has a much smaller area than the LD chip. A schematic illustration of the heat transfer problem of an LED and LD structure is shown in Figs. 1(c) and 1(d), respectively. As inferred from Fig. 1(c), the substrate of the LED chip conducts the heat but does not act as a heat spreader. As inferred from Fig. 1(d), the substrate of the LD chip acts as a heat spreader.

Because electrical RC circuits and thermal conduction are governed by mathematically identical equations, an electrothermal analogy is widely used in heat conduction analysis.⁹ This analogy allows one to apply the laws of electric circuit theory to solve the heat conduction problem. In the electrothermal analogy, the heat flow is equivalent to an electric current flow; the temperature difference is equivalent to the potential difference; the thermal resistance and the thermal capacitance are equivalent to the electrical resistance and the electrical capacitance, respectively.

Next, we will consider two cases. In the first case, corresponding to an LED, the heat source covers the entire substrate ($r_{\text{heat}} = r_{\text{substrate}}$). In the second case, corresponding to an LD, the heat source is much smaller than the substrate ($r_{\text{heat}} \ll r_{\text{substrate}}$).

Case I (LED): $r_{\text{heat}} = r_{\text{substrate}}$ The heat transfer structure is shown in Fig. 1(c) and it can be modeled by a one-dimensional (1D) structure using an $R_{\text{th}}C_{\text{th}}$ circuit with a thermal resistor and a thermal capacitor in series. Thus the thermal time constant of the heating or cooling process for a 1D material can be expressed as:

$$\tau_{\text{th}} = R_{\text{th}}C_{\text{th}}, \quad (1)$$

where R_{th} and C_{th} are the thermal resistance and the thermal capacitance of the 1D substrate material, respectively. Equa-

tion (1) gives the thermal response time for a 1D material after the power is switched on or switched off. The 1D thermal resistance of a substrate is given by:

$$R_{\text{th}} = \frac{d_{\text{substrate}}}{k_{\text{th}}A_{\text{substrate}}}, \quad (2)$$

where $d_{\text{substrate}}$ is the thickness of the substrate along the heat transfer direction, $A_{\text{substrate}}$ is the cross-section area of the substrate, and k_{th} is the thermal conductivity of the substrate material. The thermal capacitance of the 1D substrate material is given by:

$$C_{\text{th}} = c_{\text{th}}\rho d_{\text{substrate}}A_{\text{substrate}}, \quad (3)$$

where c_{th} is the thermal capacitance per unit mass (specific heat) and ρ is the mass density of the substrate material. For sapphire, $k_{\text{th}} = 0.350 \text{ W cm}^{-1} \text{ K}^{-1}$, $c_{\text{th}} = 0.760 \text{ J g}^{-1} \text{ K}^{-1}$, and $\rho = 3.98 \text{ g cm}^{-3}$; for GaN, $k_{\text{th}} = 1.30 \text{ W cm}^{-1} \text{ K}^{-1}$, $c_{\text{th}} = 0.490 \text{ J g}^{-1} \text{ K}^{-1}$, and $\rho = 6.15 \text{ g cm}^{-3}$. The thermal time constant of the 1D substrate material is approximately given by:

$$\tau_{\text{th}} \approx R_{\text{th}}C_{\text{th}} = \frac{c_{\text{th}}\rho}{k_{\text{th}}}d_{\text{substrate}}^2. \quad (4)$$

This simple, approximate result is close to the exact result of the thermal time constant (also called thermal penetration time), which can be obtained by an analytical calculation:⁴

$$\tau_{\text{th}} = \frac{\pi}{4} \frac{c_{\text{th}}\rho}{k_{\text{th}}}d_{\text{substrate}}^2. \quad (5)$$

Comparison of Eqs. (4) and (5) indicates that the thermal time constant derived from the $R_{\text{th}}C_{\text{th}}$ circuit is a good approximation of the transient response for the heating and cooling process.

It is found from Eq. (4) that the thermal time constant for the 1D substrate material does not depend on $A_{\text{substrate}}$. For a GaInN LED chip with a $200 \mu\text{m}$ thick sapphire substrate, the thermal time constant, calculated from Eq. (4), is 3.5 ms. It was reported in Ref. 10 that the thermal time constant for GaInN LEDs on a sapphire substrate is 1–2 ms. Ref. 4 re-

ported $\tau_{th}=0.72$ ms for an GaAs LED on a GaAs substrate with parameters: $c_{th}=0.327$ J g⁻¹ K⁻¹, $\rho=5.32$ g cm⁻³, $k_{th}=0.55$ W cm⁻¹ K⁻¹, and $d_{substrate}=170$ μ m, while our calculated thermal time constant for this case is $\tau_{th}=0.91$ ms. It can therefore be concluded that the thermal time constants of LEDs is on the order of a ms.

Case II (LD): $r_{heat} \ll r_{substrate}$ When the heat source radius $r_{heat} \ll r_{substrate}$, which is the case shown in Fig. 1(d), the thermal resistance of the device is given by the thermal spreading resistance. The analytical calculation of the spreading resistance is not an easy problem. However, the asymptotic solution can be obtained when $r_{heat} \ll d_{substrate}$ and $r_{heat} \gg d_{substrate}$. The heat transfer problem can be described by the Laplace equation in cylindrical coordinates (r , and z):

$$\frac{\partial^2 u}{\partial r^2} + \frac{1}{r} \frac{\partial u}{\partial r} + \frac{\partial^2 u}{\partial z^2} = 0, \quad (6)$$

where $u(r, z)$ is the local temperature increase above the ambient temperature. The three boundary conditions are:

$$u(r < r_{heat}, z = 0) = \Delta T_0 \quad (\text{uniform temperature source}), \quad (7)$$

$$\frac{\partial u}{\partial z}(r > r_{heat}, z = 0) = 0 \quad (\text{due to symmetry}), \quad (8)$$

$$u(r, z = d_{substrate}) = 0, \quad (\text{the substrate bottom is at room temperature}), \quad (9)$$

where ΔT_0 is the heat source temperature increase above the ambient temperature.

When $r_{heat} \ll d_{substrate}$ (LD case), we can simplify the problem by assuming that the substrate is infinitely thick ($d_{substrate} \rightarrow \infty$); this assumption will not significantly change the temperature distribution in the substrate near the heat source. The third boundary condition, at the bottom of the substrate, then becomes:

$$u(r, z = \infty) = 0. \quad (10)$$

Using the boundary conditions of Eqs. (7), (8), and (10), the differential Eq. (6) can be solved using Hankel transform.¹¹ The solution is in the form of an integral of Bessel function. By applying the oblate spheroid coordinate transformation:

$$z = \alpha\beta, \quad (11)$$

and

$$r = \sqrt{(1 - \alpha^2)(1 + \beta^2)}, \quad (12)$$

and then using the finite Legendre transform, the solution of the temperature distribution is obtained in a very simple form:¹²

$$u = \frac{2\Delta T_0}{\pi} \operatorname{arccot} \beta. \quad (13)$$

This equation indicates that the isothermal surfaces are semiellipsoids. The thermal spreading resistance is then obtained:

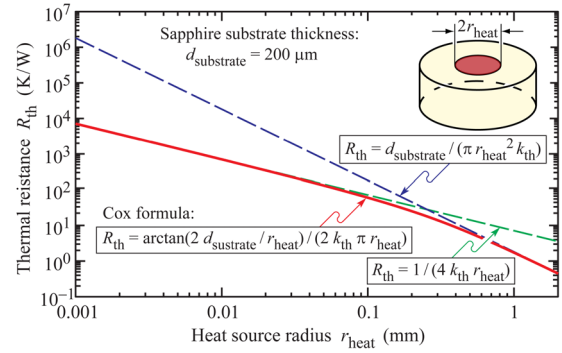


FIG. 2. (Color online) Thermal spreading resistance as a function of heat source radius for a circular heat source located on a substrate; two dashed lines are approximations for two limiting cases (green curve for $r_{heat} \ll d_{substrate}$ and blue curve for $r_{heat} \gg d_{substrate}$).

$$R_{th,spread} = \frac{\Delta T_0}{P_z} = \frac{1}{4k_{th}r_{heat}}, \quad (14)$$

where P_z is the thermal power flow from the heat source to the substrate. P_z is calculated from the integration of the thermal flow in the z direction over the whole heat source area. Note that Eq. (14) has the same form as the formula for the *electrical* spreading resistance of a circular electric contact.¹³

When $r_{heat} \gg d_{substrate}$, we can approximate the problem by a 1D problem and the spreading effect can be neglected. When r_{heat} is in between the two limiting cases, the analytical calculation is either in the form of an infinite series or an integral of Bessel functions.^{11,12,14,15} Cox and Strack obtained an empirical formula for the spreading resistance by an electrolytic tank measurement:¹³

$$R_{th,spread} = \frac{1}{2k_{th}\pi r_{heat}} \arctan\left(\frac{2d_{substrate}}{r_{heat}}\right). \quad (15)$$

Figure 2 shows the thermal spreading resistance as a function of the heat source radius; a sapphire substrate thickness of $d_{substrate}=200$ μ m is assumed. The two dashed lines are analytical approximations for the two limiting cases: $r_{heat} \ll d_{substrate}$ and $r_{heat} \gg d_{substrate}$.

The thermal capacitance of the substrate in Fig. 1(d) can be determined by using the effective heating volume of the substrate. When $r_{heat} \ll d_{substrate}$, the isothermal surfaces are semiellipsoids. Defining the spreading length r_{spread} by:

$$u(r = r_{spread}, z = 0) = \frac{1}{e} \Delta T_0 \quad (e = 2.718), \quad (16)$$

and the spreading depth d_{spread} by

$$u(r = 0, z = d_{spread}) = \frac{1}{e} \Delta T_0, \quad (17)$$

yields

$$r_{spread} = r_{heat} \sqrt{\cot^2 \frac{\pi}{2e} + 1} = 1.83r_{heat}, \quad (18)$$

and

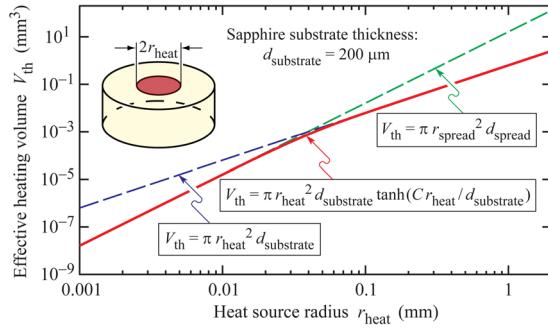


FIG. 3. (Color online) Effective heating volume with respect to heat source radius for a circular heat source located on a substrate; two dashed lines are approximations for two limiting cases (green curve for $r_{\text{heat}} \leq d_{\text{substrate}}$ and blue curve for $r_{\text{heat}} \geq d_{\text{substrate}}$).

$$d_{\text{spread}} = r_{\text{heat}} \cot \frac{\pi}{2e} = 1.53 r_{\text{heat}}. \quad (19)$$

Then the effective heated volume is given by:

$$V_{\text{th}} = \pi r_{\text{spread}}^2 d_{\text{spread}} \quad (\text{valid for } r_{\text{heat}} \leq d_{\text{substrate}}). \quad (20)$$

When $r_{\text{heat}} \geq d_{\text{substrate}}$, the spreading effect can be neglected. Therefore, the heating volume of the substrate is the volume underneath the heat source:

$$V_{\text{th}} = \pi r_{\text{heat}}^2 d_{\text{substrate}} \quad (\text{valid for } r_{\text{heat}} \geq d_{\text{substrate}}). \quad (21)$$

We can construct the following equation that asymptotically approaches these two limiting cases:

$$V_{\text{th}} = \pi r_{\text{heat}}^2 d_{\text{substrate}} \tanh\left(\frac{C r_{\text{heat}}}{d_{\text{substrate}}}\right), \quad (22)$$

where C is a constant given by:

$$C = \frac{r_{\text{spread}}^2 d_{\text{spread}}}{r_{\text{heat}}^3} = 5.12. \quad (23)$$

Thus,

$$C_{\text{th}} = c_{\text{th}} \rho V_{\text{th}} = c_{\text{th}} \rho \pi r_{\text{heat}}^2 d_{\text{substrate}} \tanh\left(\frac{C r_{\text{heat}}}{d_{\text{substrate}}}\right). \quad (24)$$

The effective heating volume as a function of radius of the heat source is shown in Fig. 3. When $r_{\text{heat}} \leq d_{\text{substrate}}$, the effective heating volume depends only on the radius of the heat source. When $r_{\text{heat}} \geq d_{\text{substrate}}$, the effective heating volume depends on both the radius of the heat source and the thickness of the substrate.

Using Eq. (15) for R_{th} and Eq. (24) for C_{th} , the thermal time constant is:

$$\begin{aligned} \tau_{\text{th}} &= R_{\text{th}} C_{\text{th}} \\ &= r_{\text{heat}} d_{\text{substrate}} \tanh\left(\frac{C r_{\text{heat}}}{d_{\text{substrate}}}\right) \arctan\left(\frac{2 d_{\text{substrate}}}{r_{\text{heat}}}\right) \frac{\rho c_{\text{th}}}{2 k_{\text{th}}}. \end{aligned} \quad (25)$$

Figure 4 shows the thermal time constant calculated from Eq. (25) as a function of the heat source radius. Inspection of the figure reveals that for a sapphire substrate thickness of 200 μm , the thermal time constant varies from microsecond to ms when the heat source radius varying from 1 μm to 1

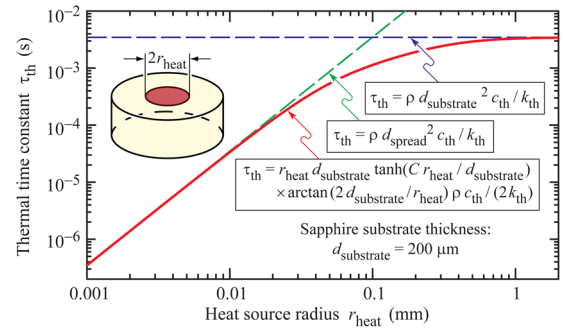


FIG. 4. (Color online) Thermal time constant as a function of heat source radius for a circular heat source located on a substrate; the two dashed lines are approximations for two limiting cases (green curve for $r_{\text{heat}} \leq d_{\text{substrate}}$ and blue curve for $r_{\text{heat}} \geq d_{\text{substrate}}$).

mm. For a GaInN LD with sapphire substrate and a circular active region with a radius of 5 μm , the thermal time constant is about 8 μs , as obtained from Fig. 4. This time is on the same order of magnitude (μs) as the simulated result reported in Ref. 16. For a GaAs LD with GaAs substrate and the same active region radius, the thermal time constant is about 3 μs as inferred from Eq. (25). This result agrees very well with values reported in the literature, which are on the order of 1 μs .^{6,17} Thus, the thermal time constants of LDs with small circular active regions ($r_{\text{heat}} = 5\text{--}10 \mu\text{m}$) and linear stripe active regions are about 0.5–5 μs (Refs. 6, 16, and 17) and 5–10 μs ,^{7,18} respectively.

III. MULTIPLE THERMAL TIME CONSTANT MODEL

The thermal structure of a packaged LED can be modeled as a multistage $R_{\text{th}}C_{\text{th}}$ circuit. In this model, each thermal component of the LED is considered as a lumped $R_{\text{th}}C_{\text{th}}$ stage. A typical flip-chip LED structure with its $R_{\text{th}}C_{\text{th}}$ model is shown in Fig. 5. The equivalent circuit is a π network (Cauer network). This network is appropriate for heat flow problems, since heat is ultimately flowing to the ambient.¹⁰ We note that this is not the case for a Foster network¹⁹ which was claimed to violate the energy conservation law.¹⁹ In the $\pi R_{\text{th}}C_{\text{th}}$ network, the first $R_{\text{th}}C_{\text{th}}$ stage is associated with the LED chip and the chip-to-submount thermal interface mate-

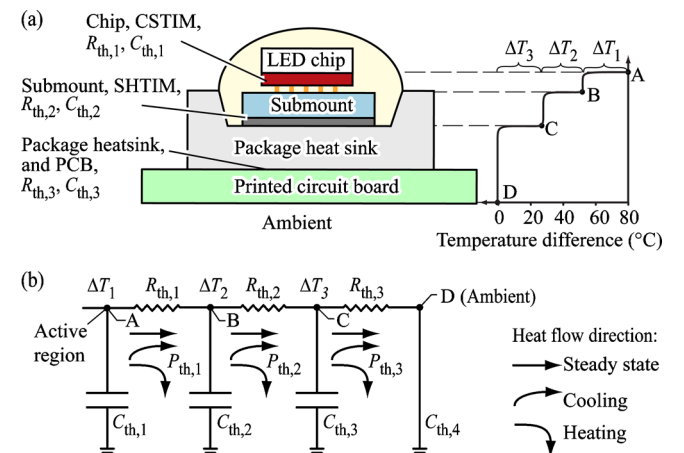


FIG. 5. (Color online) (a) A typical LED structure and its temperature distribution. (b) Corresponding multistage $R_{\text{th}}C_{\text{th}}$ model of the LED.

rial (CSTIM). CSTIM is composed of gold bumps connecting the chip and the Si submount. In the first stage, the thermal resistance is $R_{th,1}=R_{th,chip}+R_{th,CSTIM}$ and the thermal capacitance $C_{th,1}=C_{th,chip}$. The thermal capacitance of CSTIM is ignored due to the small volume of the gold bumps compared with that of the LED chip. The second $R_{th}C_{th}$ stage is associated with the submount and the submount-to-heat-sink thermal interface material (SHTIM). The SHTIM has a much smaller volume than that of the Si submount. Thus, $R_{th,2}=R_{th,Submount}+R_{th,SHTIM}$ and $C_{th,2}=C_{th,submount}$. The third $R_{th}C_{th}$ stage is associated with the package heat sink and the printed circuit board (PCB). And we have $R_{th,3}=R_{th,heat\ sink+PCB}+R_{th,convection}$ and $C_{th,3}=C_{th,heat\ sink+PCB}$. We note that Fig. 5 shows no capacitor between the PCB and the ambient. This is due to the fact that the ambient has an infinitely large thermal capacitance. We can represent an infinitely large capacitor by a short circuit since:

$$Z_{th} = \frac{1}{i\omega C_{th}} \rightarrow 0 \quad \text{for} \quad C_{th} \rightarrow \infty. \quad (26)$$

Székely¹⁹ showed by network transformation that the transient thermal response, after power is switched off, can be expressed by a sum of exponential terms:

$$\Delta T = \sum_{i=1}^n \Delta T_i \exp\left(-\frac{t}{\tau_{th,i}}\right). \quad (27)$$

Note that for the general case, the thermal time constant $\tau_{th,i}$ is not simply $\tau_{th,i}=R_{th,i}C_{th,i}$ but is determined by the whole $R_{th}C_{th}$ circuit. However, in typical LED structures, the thermal capacitances usually satisfy the following relation:

$$C_{th,1} \ll C_{th,2} \ll C_{th,3} \ll C_{th,4}. \quad (28)$$

This is because the volume of the component associated with each thermal capacitance becomes increasingly bigger (LED chip, Si submount, heat sink, PCB board, etc.). On the other hand, for a reasonable design of an LED, the thermal resistances of different stages should be on the same order of magnitude, that is,

$$R_{th,1} \approx R_{th,2} \approx R_{th,3} \approx R_{th,4}, \quad (29)$$

so that there is no ‘‘bottleneck’’ effect that would strongly impede the heat flow. Thus, we have,

$$R_{th,1}C_{th,1} \ll R_{th,2}C_{th,2} \ll R_{th,3}C_{th,3} \ll R_{th,4}C_{th,4}. \quad (30)$$

With this condition, it will be proven in the Appendix that the time constant of each exponential term is approximately equal to $\tau_{th,i}=R_{th,i}C_{th,i}$. Schematic illustrations of the junction temperature decay on linear time scale and logarithmic time scale are shown in Figs. 6(a) and 6(b), respectively. Figure 6(b) shows that using logarithmic time scale allows one to distinguish between the different thermal time constants. The distinct dependence of ΔT on t , particularly the occurrence of flat regions [$d\Delta T/d \log(t)=0$] and the occurrence of strongly sloped regions [$d\Delta T/d \log(t) \neq 0$] can be used to determine the time constants of specific stages and their associated components.

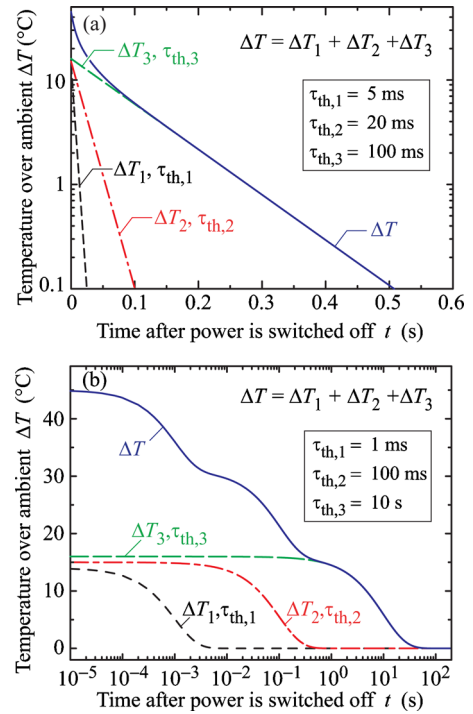


FIG. 6. (Color online) Schematic junction temperature decay having three exponential decay terms after the power is switched off at $t=0$ on (a) a linear time scale and (b) a logarithmic time scale.

The temperature response after the power is switched on can be qualitatively explained as follows: in the initial stage, the LED chip is heated up in a very short time. Since $C_{th,i>1} \gg C_{th,1}$, the thermal capacitors in the following stages can be considered as a short-circuit connection to the ground.²⁰ Therefore, the thermal time constant $\tau_{th,1} = R_{th,1}C_{th,1}$. Subsequently the submount starts to heat up and this is governed by a much longer thermal time constant, which is dominated by the second $R_{th}C_{th}$ stage; and so on. The transient cooling process can be considered to be analogous to the heating process.

IV. EXPERIMENTAL PROCEDURES USED IN THE TRANSIENT JUNCTION TEMPERATURE MEASUREMENT

The device under test is a high-power flip-chip LED with emission at 395 nm. The structure of the LED package is shown in Fig. 7. The LED is grown on sapphire substrate by metal-organic vapor-phase epitaxy. The LED consists of a

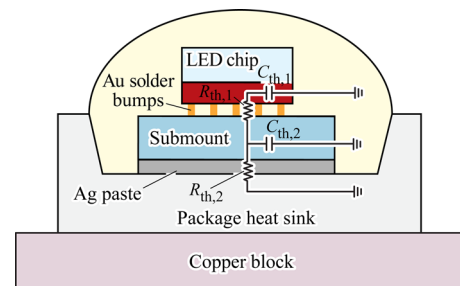


FIG. 7. (Color online) Packaged LED structure consisting of LED chip, submount, and package and its thermal $R_{th}C_{th}$ model.

2 μm thick undoped GaN layer, a 3 μm Si-doped GaN layer, six-period Si-doped GaInN/GaN multiple quantum wells, a 24 nm Mg-doped AlGaIn electron blocking layer, a 100 nm Mg-doped p-type GaN, and a 45 nm Mg-doped p⁺-type GaN layer. The LED chip is mounted on the silicon submount via CSTIM, i.e., the gold bumps. The submount has a dimension of $2 \times 2 \times 0.4 \text{ mm}^3$. The SHTIM, which is made of silver paste, is used to attach the submount and the heat sink. The heat sink is made of copper coated with aluminum.

In our experiments, the measurement method for the junction temperature is the forward-voltage method.² This method includes two steps. In the first step, the sample is placed in a temperature controlled oven. For different oven temperatures, the forward voltage is measured at an injection current of 10 mA, which is the “probe current” to be used in the second step. The probe current is low enough so that the junction temperature remains the same as the oven temperature. In the second step, the forward voltage of the device is measured at the probe current. The junction temperature of the device is then determined by using the calibration data obtained in the first step.

By a linear fit of the V_f versus T_{oven} curve from the first step, the temperature coefficient dV_f/dT is obtained for a probe current of 10 mA. For our measurement, the temperature coefficient is determined to be -1.84 mV/K , which is in a good agreement with the theoretical calculation reported in Ref. 2. In the transient junction temperature measurement, we attach the LED package to a large copper block so that the temperature of the package heat sink is at room temperature. Currents with pulse duration of 200 ms (i.e., quasi-dc) and period of 1 s are injected into the sample. The currents vary from 200 to 800 mA with an increment of 100 mA. 200 ms is experimentally proven to be much longer than the time required for heating the device to the steady state. During the cooling period, we apply a probe current of 10 mA. This probe current does not induce significant heat to the junction and thus will not influence the temperature during cooling. The junction temperature is obtained from the calibrated forward voltage at the probe current.

V. EXPERIMENTAL RESULTS ANALYSIS

Figure 8 shows the transient junction temperature response after the power is switched off. The quasi-dc currents range between 200 and 800 mA. We use a logarithmic time scale as abscissa, which can show very different time constants in one diagram. The experimental data is fitted by a single exponential function as well as multiexponential functions. We found that a single exponential function does not fit the experimental data well. Therefore, we fit the experimental results by the following function which has two exponential terms:

$$\Delta T(t) = \Delta T_1 \exp\left(-\frac{t}{\tau_{\text{th},1}}\right) + \Delta T_2 \exp\left(-\frac{t}{\tau_{\text{th},2}}\right). \quad (31)$$

Four fitting parameters are used to fit the equation to the experimental data: ΔT_1 , ΔT_2 , $\tau_{\text{th},1}$, and $\tau_{\text{th},2}$. The theoretical fits are also shown in Fig. 8. Inspection of the figure reveals

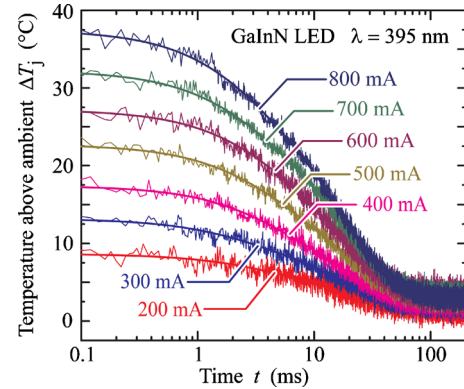


FIG. 8. (Color online) Measured temperature decay curves for different drive currents of a GaInN LED. The LED drive current is switched off at $t=0$. The solid lines are fitting curves that closely match the experimental data. The fitting curves consist of two exponential terms.

that the experimental data is fitted very well by the equation.

The four fitting parameters as a function of current are shown in Fig. 9. It is found that ΔT_1 and ΔT_2 monotonically increase with current. However, the ratio of ΔT_2 and ΔT_1 does not change much with current. The average value of $\Delta T_2/\Delta T_1$ is about 3.3. Moreover, $\tau_{\text{th},1}$ and $\tau_{\text{th},2}$ vary little with current. By averaging the thermal time constants over different currents, we obtain the two thermal time constants: $\tau_{\text{th},1} = 2.72 \text{ ms} \pm 0.68 \text{ ms}$ and $\tau_{\text{th},2} = 18.8 \text{ ms} \pm 0.8 \text{ ms}$. This indicates that, as expected, the thermal properties of the LED are determined by the thermal resistance and the thermal capacitance of the materials and not by the input power. The two time constants obtained from the fitting, $\tau_{\text{th},1}$ and $\tau_{\text{th},2}$, are considered as the times required for cooling down (or heating up) the chip and the submount, respectively.

Figure 10 shows the steady-state junction temperature at $t \leq 0$ (before the power is switched off) versus the input power. The linear fit of the junction temperature versus the input power yields an approximate thermal resistance of 12.2 K W^{-1} from the chip to the package heat sink. From Eqs. (A12), (A13) and (A14), the following fitting parameters of the two stage $R_{\text{th}}C_{\text{th}}$ circuit are extracted: $R_{\text{th},1} = 2.83 \text{ K W}^{-1}$, $R_{\text{th},2} = 9.39 \text{ K W}^{-1}$, $C_{\text{th},1} = 0.962 \text{ mJ K}^{-1}$ and $C_{\text{th},2} = 2.00 \text{ mJ K}^{-1}$. The calculated thermal capacitances of the chip and the Si submount are 0.652 mJ K^{-1} (chip: V

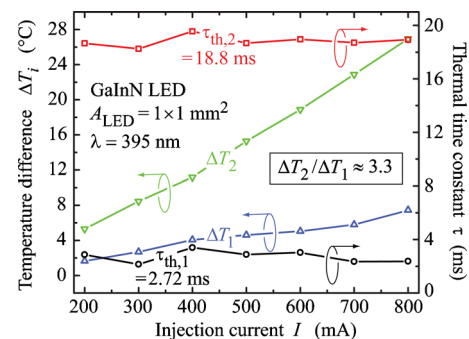


FIG. 9. (Color online) Measured temperature differences between active region and submount (ΔT_1) and submount and package heat sink (ΔT_2) of a packaged GaInN LED as a function of the injection current. Also shown are the associated thermal time constants, as extracted from the temperature decay curves.

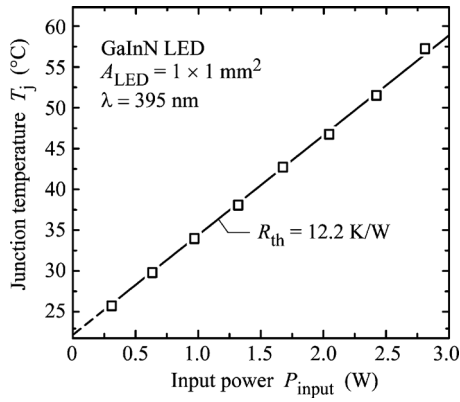


FIG. 10. Measured junction temperature of a GaInN LED vs input power using the forward-voltage method.

$=1 \times 1 \times 0.2 \text{ mm}^3$, $\rho=3.98 \text{ g cm}^{-3}$, $c_{\text{th}}=0.760 \text{ J g}^{-1} \text{ K}^{-1}$) and 2.66 mJ K^{-1} (submount: $V=2 \times 2 \times 0.4 \text{ mm}^3$, $\rho=2.33 \text{ g cm}^{-3}$, $c_{\text{th}}=0.713 \text{ J g}^{-1} \text{ K}^{-1}$), respectively. Comparing the two calculated thermal capacitances to the two thermal capacitances obtained from the fitting, it is straightforward to identify $C_{\text{th},1}$ as the thermal capacitance of the LED chip and $C_{\text{th},2}$ as the thermal capacitance of the Si submount. The gold bumps connecting the chip and the submount have a high bulk thermal conductivity. However, the effective contact area of the sandwiched gold bumps between the submount and the chip epilayer is determined by the pressure during the coining process. This effective contact area could be much smaller than the cross section of the LED chip. Therefore the thermal resistance of the gold bumps cannot be neglected. $R_{\text{th},1}$ is then composed of the gold bumps as well as the sapphire substrate. $R_{\text{th},2}$ is caused by the thermal resistance of the Si submount and the contact thermal resistance between the submount and the package heat sink.

Based on the above discussions, we come to the conclusion that the transient response of the junction temperature can be expressed as a multiexponential function. Two thermal time constants are determined and found to be on the order of 2 and 20 ms, and they are associated with the LED chip and the LED Si submount, respectively.

VI. CONCLUSIONS

We analyze the thermal properties, including the thermal time constants, of unpackaged LEDs and unpackaged LDs at the chip level. The thermal properties of LED chips are described by a single thermal time constant, which is associated with the substrate. For LD chips, a heat spreading volume is introduced to determine the thermal time constant. The thermal properties of LD chips are described by the single thermal time constant associated with the heat spreading volume in the substrate. The calculation shows that the thermal time constant for LED chips is on the order of ms; and for LD chips, it is on the order of microsecond. We develop an $R_{\text{th}}C_{\text{th}}$ network model for packaged LEDs. Using this model, the transient junction temperature can be described by a multiexponential function. Each time constant of this function is approximately the product of the thermal resistance, R_{th} , and the thermal capacitance, C_{th} , of each

stage. The transient response of a high-power flip-chip LED is measured by the forward-voltage method. The fitting of the experimental results reveals two thermal time constants, which are 2.72 ms and 18.8 ms and associated with the LED GaInN/sapphire chip and LED Si submount, respectively.

ACKNOWLEDGMENTS

The RPI authors gratefully thank Samsung LED, National Science Foundation, New York State, Crystal IS, Troy Research Corporation, and Sandia National Laboratory's Solid-State Lighting Science Center, an Energy Frontiers Research Center funded by the U.S. Department of Energy, Office of Science, and Office of Basic Energy Sciences. The authors would also like to thank Mr. John Schatz for expert technical assistance.

APPENDIX

In this appendix, we derive the junction temperature decay as a function of time after the power is switched off at $t=0$. We first consider a single $R_{\text{th}}C_{\text{th}}$ circuit. The time dependent junction temperature after the current is switched off is given by:

$$\Delta T = \Delta T_0 \exp\left(-\frac{t}{\tau_{\text{th}}}\right), \quad (\text{A1})$$

where ΔT_0 is the difference between junction temperature and ambient temperature at $t=0$, and $\tau_{\text{th}}=R_{\text{th}}C_{\text{th}}$. A two stage $R_{\text{th}}C_{\text{th}}$ network is shown in Fig. 7. By using Kirchoff's current law and Ohm's law, we find that the governing equation for ΔT is a second order differential equation:

$$\frac{d^2\Delta T(t)}{dt^2} + \left(\frac{1}{R_{\text{th},2}C_{\text{th},2}} + \frac{1}{R_{\text{th},1}C_{\text{th},2}} + \frac{1}{R_{\text{th},1}C_{\text{th},1}}\right) \frac{d\Delta T(t)}{dt} + \frac{1}{R_{\text{th},1}C_{\text{th},1}R_{\text{th},2}C_{\text{th},2}} \Delta T(t) = 0. \quad (\text{A2})$$

This differential equation is of the form: $y(x)'' + Ay(x)' + By(x) = 0$. The characteristic equation of this homogeneous differential equation is:

$$\left(\frac{1}{\tau_{\text{th}}}\right)^2 - \left(\frac{1}{R_{\text{th},2}C_{\text{th},2}} + \frac{1}{R_{\text{th},1}C_{\text{th},2}} + \frac{1}{R_{\text{th},1}C_{\text{th},1}}\right) \frac{1}{\tau_{\text{th}}} + \frac{1}{R_{\text{th},1}C_{\text{th},1}R_{\text{th},2}C_{\text{th},2}} = 0. \quad (\text{A3})$$

This is a quadratic equation and the two solutions of τ_{th} must satisfy the conditions:

$$\frac{1}{\tau_{\text{th},1}} + \frac{1}{\tau_{\text{th},2}} = \frac{1}{R_{\text{th},2}C_{\text{th},2}} + \frac{1}{R_{\text{th},1}C_{\text{th},2}} + \frac{1}{R_{\text{th},1}C_{\text{th},1}}, \quad (\text{A4})$$

and

$$\frac{1}{\tau_{\text{th},1}\tau_{\text{th},2}} = \frac{1}{R_{\text{th},1}C_{\text{th},1}R_{\text{th},2}C_{\text{th},2}}. \quad (\text{A5})$$

Using

$$C_{\text{th},2} \gg C_{\text{th},1}, \quad (\text{A6})$$

and

$$R_{th,2} \approx R_{th,1}, \quad (A7)$$

we obtain:

$$\begin{aligned} \left(\frac{1}{\tau_{th,1}} + \frac{1}{\tau_{th,2}} \right)^2 &= \left(\frac{1}{R_{th,2}C_{th,2}} + \frac{1}{R_{th,1}C_{th,2}} + \frac{1}{R_{th,1}C_{th,1}} \right)^2 \\ &\approx \left(\frac{1}{R_{th,1}C_{th,1}} \right)^2 = \frac{1}{R_{th,1}C_{th,1} R_{th,1}C_{th,1}} \\ &\gg \frac{1}{R_{th,1}C_{th,1} R_{th,2}C_{th,2}} = \frac{1}{\tau_{th,1} \tau_{th,2}}. \end{aligned} \quad (A8)$$

Therefore

$$\left(\frac{1}{\tau_{th,1}} + \frac{1}{\tau_{th,2}} \right)^2 \gg \frac{1}{\tau_{th,1} \tau_{th,2}}. \quad (A9)$$

If the two capacitances are very different, we can write

$$\left(\frac{1}{\tau_{th,1}} + \frac{1}{\tau_{th,2}} \right)^2 \gg 4 \frac{1}{\tau_{th,1} \tau_{th,2}}. \quad (A10)$$

If the two time constants were the same, then both sides of the equation would be identical. However, since the inequality mandates that the two sides are very different, it implies that the two time constants are very different from each other. Therefore we assume:

$$\tau_{th,2} \gg \tau_{th,1}. \quad (A11)$$

From Eq. (A4) and using Eq. (A6), we obtain

$$\frac{1}{\tau_{th,1}} \approx \frac{1}{R_{th,2}C_{th,2}} + \frac{1}{R_{th,1}C_{th,2}} + \frac{1}{R_{th,1}C_{th,1}} \approx \frac{1}{R_{th,1}C_{th,1}}. \quad (A12)$$

Furthermore, by using Eq. (A5), we obtain:

$$\frac{1}{\tau_{th,2}} \approx \frac{1}{R_{th,2}C_{th,2}}. \quad (A13)$$

Using Eqs. (A12) and (A13), the solution of Eq. (A2) can be written as:

$$\Delta T(t) = \Delta T_1 \exp\left(-\frac{t}{\tau_{th,1}}\right) + \Delta T_2 \exp\left(-\frac{t}{\tau_{th,2}}\right), \quad (A14)$$

where ΔT_1 and ΔT_2 are the steady-state temperature drops across $R_{th,1}$ and $R_{th,2}$, respectively.

For an $R_{th}C_{th}$ network with the number of stages greater than 2, we can make the following approximation during the cooling down (or heating up) of the i th stage: The impedance of the j th capacitor ($j > i$) is given by

$$Z_{th,j} = \frac{1}{i\omega C_{th,j}} \rightarrow 0, \quad \text{when } C_{th,j} \gg C_{th,i}. \quad (A15)$$

Therefore, we approximate the capacitor after the i th stage, i.e., the j th stage, as short-circuit connection to ground. Therefore, the contribution of C_j on the cooling of the i th stage can be neglected. Then the time constant of the i th RC cell is just

$$\tau_{th,i} \approx R_{th,i}C_{th,i}. \quad (A16)$$

Furthermore, the temperature decay function can be written as:

$$\Delta T(t) = \sum_{i=1}^n \Delta T_i \exp\left(-\frac{t}{\tau_{th,i}}\right). \quad (A17)$$

The heating transient response has the same characteristic equation of the thermal time constant as Eq. (A3). This indicates that the heating response function is given by:

$$\Delta T(t) = \sum_{i=1}^n \Delta T_i \left[1 - \exp\left(-\frac{t}{\tau_{th,i}}\right) \right]. \quad (A18)$$

¹E. F. Schubert, *Light-Emitting Diodes*, 2nd ed. (Cambridge University Press, Cambridge, 2006).

²Y. Xi and E. F. Schubert, *Appl. Phys. Lett.* **85**, 2163 (2004).

³Y. Xi, J.-Q. Xi, Th. Gessmann, J. M. Shah, J. K. Kim, E. F. Schubert, A. J. Fischer, M. H. Crawford, K. H. A. Bogart, and A. A. Allerman, *Appl. Phys. Lett.* **86**, 031907 (2005).

⁴N. C. Chen, Y. K. Yang, Y. N. Wang, and Y. C. Huang, *Appl. Phys. Lett.* **90**, 181104 (2007).

⁵P. Vitta and A. Žukauskas, *Appl. Phys. Lett.* **93**, 103508 (2008).

⁶G. Hasnain, K. Tai, L. Yang, Y. H. Wang, R. J. Fischer, J. D. Wynn, B. Weir, N. K. Dutta, and A. Y. Cho, *IEEE J. Quantum Electron.* **27**, 1377 (1991).

⁷C. Eichler, S.-S. Schad, M. Seyboth, F. Habel, M. Scherer, S. Miller, A. Weimar, A. Lell, V. Härle, and D. Hofstetter, *Phys. Status Solidi C* **7**, 2283 (2003).

⁸Z. Gong, M. Gaevski, V. Adivarahan, W. Sun, M. Shatalov, and M. Asif Khan, *Appl. Phys. Lett.* **88**, 121106 (2006).

⁹V. S. Arpaci, *Conduction Heat Transfer* (Addison-Wesley, Reading, Massachusetts, 1966).

¹⁰P. Vitta and A. Žukauskas, *Phys. Status Solidi C* **6**, S877 (2009).

¹¹I. N. Sneddon, *Mixed Boundary Value Problems in Potential Theory* (Wiley, New York, 1966).

¹²C. J. Tranter, *Integral Transforms in Mathematical Physics* (Wiley, New York, 1966).

¹³R. H. Cox and H. Strack, *Solid-State Electron.* **10**, 1213 (1967).

¹⁴B. Belmont and M. Shur, *Solid-State Electron.* **36**, 143 (1993).

¹⁵M. W. Denhoff, *J. Phys. D* **39**, 1761 (2006).

¹⁶J. Piprek, *Proc. SPIE* **6013**, 60130B (2005).

¹⁷P. V. Mena, J. J. Morikuni, S.-M. Kang, A. V. Harton, and K. W. Wyatt, *J. Lightwave Technol.* **17**, 865 (1999).

¹⁸R. D. Esman and D. L. Rode, *J. Appl. Phys.* **59**, 407 (1985).

¹⁹V. Székely, *Microelectron. J.* **28**, 277 (1997).

²⁰F. N. Masana, *Microelectron. Reliab.* **41**, 901 (2001).